Measurement of stress and strain development around a pile in a photoelastic granular material

Dijkstra, J.; Broere, W.; Van Tol, A. F.

Publication date
2006

Document Version
Accepted author manuscript

Published in
Geomechanics and Geotechnics of Particulate Media

Measurement of stress and strain development around a pile in a photoelastic granular material

J. Dijkstra[1], W. Broere[1,2] & A.F. van Tol[1,3]
(1) Delft University of Technology, Delft, The Netherlands
(2) A.Broere BV, Amsterdam, The Netherlands
(3) GeoDelft, Delft, The Netherlands

This paper presents the results of model pile load tests in a photoelastic material. The soil in this test is represented by an assembly of photoelastically sensitive glass particles. This allows for the determination of stresses in the assembly by the photoelastic method. Displacements around the pile are measured using digital image correlation. Tests were performed in a medium dense particle assembly. The development of stresses and strains, in particular the development of horizontal stress, around the pile tip and pile shaft are quantified and presented in this paper.

1 INTRODUCTION

Displacement piles, such as concrete prefabricated piles, are often used for pile foundations. During the installation of a displacement pile the soil around the pile is pushed away and distorted. For a driven pile the process is even more complex, due to vibrations caused by the installation process. In engineering practice the installation effects are accounted for in the empirical design method. However, when the modelling of pile foundations is attempted in finite element code, the installation phase is often not taken into account. The occurrence of large strains and the limited knowledge of the material behaviour around a displacement pile complicate the calculations and leads to large differences between predictions and measurements.

The tests presented in this paper are part of a more extensive research effort in which the soil behaviour around a displacement pile in sand is investigated during jacked installation. The goal is to quantify the change of strength and stiffness properties of the soil near the pile, due to pile installation. The objective is to formulate these as fundamental soil properties suited for constitutive models of FEM code.

Often only the displacements near a pile or a cone are measured, e.g. Davidson and Boghrat (1983) or De Pater and Nieuwenhuis (1986). Both studied the displacement near a penetrated cone with a stereo imaging technique and more recently White and Lehane (2004), studied the displacements near a jacked displacement pile by digital image correlation. Ideally, besides the measurements of the displacement field (and strain) also the stresses around the pile should be known for a better understanding of the installation process.

However, the measurement of stresses in the soil is often limited to a few point measurements taken at the boundaries of the model, or at instrumented piles. In other cases the stress is measured by transducers, which are embedded in the soil. Those transducers become rather complex when all stress components are needed. Considering the conditions in model tests, i.e. the instrumentation of model piles, the complexity of transducers is even more challenging. Another aspect is the quantification of the influence of these transducers on the measured results. Finally large amount of sensors would be needed to get a detailed stress field, this possibly leads to even larger influences on the measurements.

It is possible to obtain detailed information on the stress distribution of a granular material using the photoelastic measuring method. The soil is replaced by grains of a photoelastic material, in this case glass particles (Wakabayashi 1957, Drescher 1976). Crushed glass behaves similar to sand particles, although, the grains are more angular. Therefore it is a reasonable substitute to investigate sand behaviour.

In comparison with the photoelastic measurement methods for continuous materials the quantification of the stress paths for a granular material is hampered.

First, in order to eliminate light scatter the pores have to be filled with a liquid which has a similar refraction index as the glass particles. Secondly the analysis of the fringe patterns is impossible because of the stacked nature of the sample. Each layer of grains produces it's own fringe pattern resulting in a mix of fringes which cannot be interpreted. The first condition leads to the qualitative visualization of these stress paths by a circular polariscope, see i.e. Wakabayashi (1957). For the second problem, quantification of the stress paths, Allersma (1982) developed an automated polariscope.

2 STRESS AND STRAIN MEASUREMENTS

2.1 Stress measurements

In general, granular material does not behave elastically, as is often assumed when formulating a stress-strain relationship. Therefore it is not possible to derive the stress increments from strain measurements. The stresses have to be measured independently of the strains.

In this case the method developed by Allersma (1987) and Allersma and Broere (2002) for measurement of the stress in a photoelastic material is followed. The method developed by Allersma (1982) is most comparable to phase-stepping photoelasticity as described in e.g. Ajovalasit et al. (1998). The direction of the principal stress and the principal stress difference along the light path are measured with an automated circular polariscope. Therefore averaging of the stress in the direction normal to the plane is taken into account.

In a photoelastic material the refraction in each direction is dependent on the normal stress in that direction. The stress difference between the principal stress directions, i.e. twice the maximum shear stress, $2 * \tau_{max}$, leads to a relative velocity difference and subsequently a change in polarisation. This change in retardation can be measured to obtain the shear stress in a point.

The maximum shear stress in a point can be derived from the elliptical polarisation of the light. The light changes from circular polarised light into elliptical polarised light when travelling through the sample, caused by the stress in the material.

If at one or more points the complete stress state is known, the absolute values of the stress tensor can be determined by integrating the equilibrium equations. In the present tests the vertical stress is calculated from the measured surcharge at the top of the sample.

2.2 Strain measurements

The displacement field is obtained from two subsequent images by digital image correlation (DIC), a cross correlation algorithm. The strains are derived by mapping a rectangular grid through the displacement field and subsequently deriving the strain per element from the nodal displacements. Strains within the element are linearly interpolated using shape functions obtained from Smith and Griffiths (1998).

Although relatively new in geomechanics digital cross correlation of images has already been employed in fluid mechanics for several years. For an excellent overview is referred to Sveen and Cowen (2004). The principle can be summarized as follows: A digital image is interpreted as an intensity function at each pixel location. When for two images these functions are cross-correlated, a peak correlation value for the best matching location is found. For optimum correlation the origin of the second image has to be shifted to this new location. This shift is equal to the magnitude and direction of the displacement between the two images.

However, the image needs to have sufficient contrast in order to correlate the two images. In fluid mechanics a speckle pattern is created by illuminating tracers in the stream with a laser beam. In geomechanics enough contrast is found in the material itself if sand is used, e.g. Wolf et al. (2003) or White and Lehane (2004). For soft soils so far only substitute transparent soils in combination with a laser beam for illumination deliver the desired speckle pattern with sufficient contrast (Sadek et al. 2003).

For the model pile tests in crushed glass reported, here the DIC method succeeds because of a slight imperfection in the setup. Ideally, the refraction index of the liquid in the pores matches the refraction index of the grains. In the current setup a slight deviation between the two refraction indices is present, which allows for the use of image correlation, as the edges of the glass particles remain visible. This results in enough intensity differences in the image that the calculation of the displacement field can succeed.

The freely available MPIV toolbox for MATLAB of Mori and Chang (2003) is used for the present tests. This toolbox which originally is designed for fluid dynamics incorporates, besides the traditional cross correlation algorithm, also a minimum quadratic difference (MQD) method. The latter method is far more robust for images with lower contrast differences. It is in fact perfectly suited for the detection of movements in the glass particle assembly.

3 TEST SETUP AND TEST PROCEDURE

3.1 Test setup

The test setup consists of a strongbox with inner dimensions h x w is 400 mm x 400 mm and d = 21 mm, see Figure 1. The front and rear sides are made of glass. The pile consists of a steel strip with a thickness of 5 mm and the same width as the model depth (21 mm). An additional surcharge 'q' is applied to increase the stress level in the sample. Both the sur-

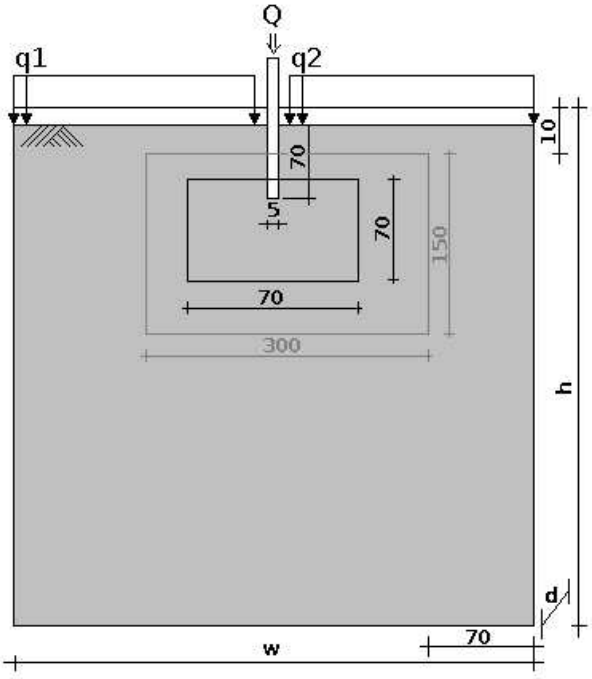

Figure 1: Front view model setup

charge and the pile head are equipped with a load cell.

The box is filled with glass particles and the liquid. The particle size of the glass particles is between 1 and 2 mm. The material behaves similar to sand of the same particle size as shown in triaxial tests performed by Allersma (Figure 2.) According to Allersma, the angle of internal friction at constant volume, ϕ_{cv}, for angular silica sand of this particle size is about 31^0 and for crushed glass about 33^0.

3.2 Test procedure

Medium dense conditions (void ratio of 0.66) are obtained by first pouring the glass into the strongbox, subsequently densification of the sample, and finally pumping the liquid through the sample from bottom to top. A surcharge of 50 kPa is applied at both sides of the pile after preparation of the sample is finished. When preparation of the sample is finished a void ratio of 0.66 is found and is normally consolidated. The pile is loaded by a computer controlled stepper motor. The effective surcharge is measured as a total load on the top of the boundary, therefore local effects, e.g. near the pile, are not measured. During the test a decrease in the total load is found. This decrease is caused by deformations, most probably creep, in the particle assembly during the lengthy measurement.

The mechanical polariscope is mounted on a computer controlled x-y scanner and scans approximately 450 stress points in an area of ca. 300 mm x 150 mm centered around the pile tip (shown in Fig.1). The computer controlled digital camera is focused on the same area of interest. The pile is installed after the sample is prepared and the surcharge is applied. After each load step of 1 mm the pile load and the surcharge are registered. Subsequently a picture for the DIC analysis is taken. The stress measurement with the polariscope is performed each 10th load increment, i.e. after 10 mm of pile displacement.

4 TEST RESULTS

The results of the test in the medium dense particle assembly (void ratio of 0.66) are given in Figs. 3. & 4. The first series of figures show the development of the principal stress around the pile and the derived stress components on the pile during the penetration. In the second series the development of strains is given. Because of the small zone of the strain development the area for which the strains are given is smaller then the area of the stress measurements. The search windows for both measurement types are given in Fig. 1. The black box covers the area for the strain measurements, the grey box is showing the search window for the stress measurements.

4.1 Stresses near the pile

From the photoelastic procedure the directions and magnitude of the principal stress are shown. Also for several stages of pile penetration the development of the reaction stress on the pile are given. In Figure 3(a), the principal stresses and their rotation after 30 mm of pile penetration are shown. Figure 3(b) & 3(c) show

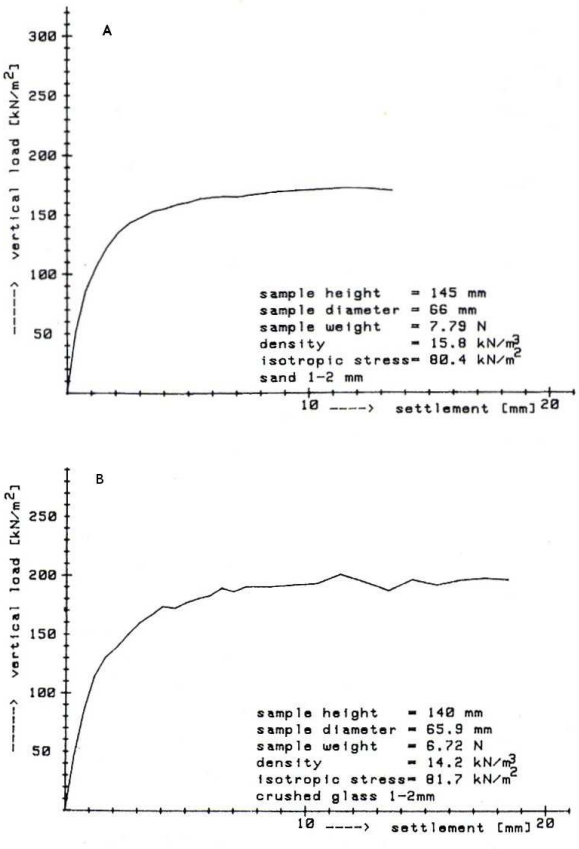

Figure 2: Triaxial test on (a) angular silica sand and (b) crushed glass (from Allersma 1987)

the stress development on the pile (extrapolated from the nearest stress point). Figure 3(b) gives for seven load stages the development of horizontal stresses after resp. 0, 10 ,20, 30, 40, 50, 60 and 70 mm of pile penetration. Figure 3(c) is similar but gives the development of horizontal stress in a point located at a certain depth.

The stress state after the first 30 mm of pile penetration is given in Figure 3(a). The pile load measured at the pile head is found to be constant from this load step. The magnitude of both the rotation and the principal stress near the shaft are given in Figure 3(a). It is interesting to note that the magnitude of τ_{max} decreases with increasing distant from the pile shaft. In other words the ratio between the primary and secondary principal stress is approximating one. Another observation is that the stresses in the by pile installation distorted assembly near the pile are much larger then below the pile tip, possibly induced by the large shear strains, but more likely by the boundary. The far field stresses are still relatively unchanged.

When is attempted to plot the horizontal stress at the pile for several load steps, Figure 3(b) is obtained. The horizontal stress is plotted for a virtual vertical cross-section next to the pile (interval of 10 mm ranging from 2 to 7 cm below surface shown in Fig. 3(a)). The situation before installation and each subsequent load stage of 10 mm are shown (horizontal stress after resp. 0, 10 ,20, 30, 40, 50, 60 and 70 mm of pile penetration). After 10 mm of pile penetration the pile tip is at the top of the graph (thus already 20 mm embedded in the assembly) and after the last load step the pile tip is at the bottom of the graph. Therefore after e.g. the 20th load step the horizontal stress at a depth of 6 cm is still unaltered. This phenomenon is better identified in Figure 3(c). Although stress changes are observed it is difficult to identify a clear tendency of stress development. The approach of the pile tip is not visible in the graph. When the development of horizontal stress in a fixed point is plotted a better overview on the stress change is found. Unfortunate the trend of the measured horizontal stress after 60 mm and 70 mm pile penetration deviate from the others and are of less qualtiy.

For six stress points spaced at 10 mm above each other on the same virtual vertical cross section next to the pile the development of the horizontal stress after respectively 0, 10, 20, 30, 40, 50, 60 and 70 mm of pile displacement is shown in Figure 3(c). Due to the spacing of the discrete stress measurements of about 10 mm, after each 10 steps of displacement (= 10 mm of pile displacement) the pile tip reaches the next stress measurement point. Clearly a stress increase of the highest stress measurement point (row1) until the 30th load step is found. The second point lags about 10 load steps behind the first point and when the third point is considered it lags 20 steps behind. After a peak value is reached (20 mm above the pile tip) a gradual decrease is observed. In comparison with other (model) pile tests this behaviour is most similar to the friction fatigue effect described by White and Lehane (2004).

The residual stress after the peak value is found to be similar to the initial after step 0, however, compared to the stress after load step 10 overall a slight increase is found.

4.2 Strains near the pile

The displacement field, volumetric strain and shear strain for the situation after 30 mm pile displacement are given in Figs. 4(a), 4(b) and 4(c). Compressive strains are chosen to be negative and due to the large pile displacement quite large in magnitude. The difference in sign of the shear strain on the left of the pile compared to the shear strain on the right of the pile stems from the sign convention. Unfortunate a lot of noise is introduced in the results, the origin of these has to be found in the relatively large displacement increments between two photographs and a shadow band which can be seen in Figure 4(a). The algorithm does not yield feasible results in this shadow band.

The displacement field shown in Figure 4(a) shows clearly a curve shaped failure pattern. Although, no clear position of a return point can be identified.

When the volumetric and shear strain (Fig. 4(b) and Fig. 4(c)) are compiled from the displacement field, one may notice that the magnitude of both quantities exceed 100 %. A closer look reveals a clear dilatant zone below the pile tip. This can be expected in initial medium dense conditions. The grains which are initially locked in place have to dilate first before they can move.

The particle assembly near the pile is heavily distorted. The influenced zone is relatively narrow, a total width of about eight pile diameters for the shear strain and a total width of about twelf pile diameters for the volumetric strain is found. Also the origin of the strain is initiated at the corner of the pile, the largest shear strain is found at the pile corner.

5 DISCUSSION

Although the results are promising, some improvements of the test setup are scheduled to improve the representation of the stress patterns around the pile. The ratio between pile diameter and particle size is now ≈ 5. The ratio should be increased to ≈ 20. The particle size is fixed therefore a bigger strongbox needs to be used in order to prevent boundary effects.

Enlarging the pile dimensions the pile can also be instrumented with several load cells. This gives additional information to corrolate the results found in this test setup with regular model tests in non-photoelastic

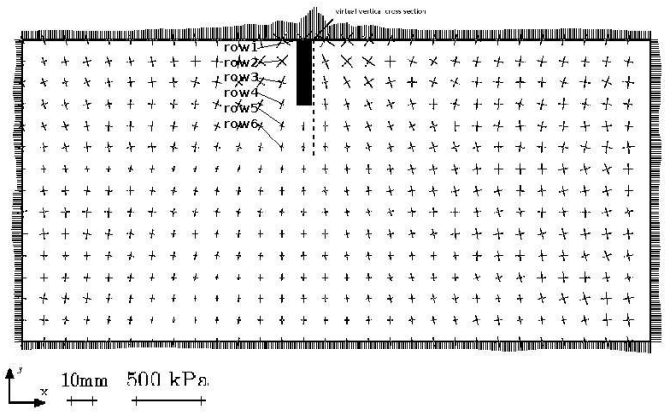

(a) Measured principal stress directions after 30 mm pile penetration

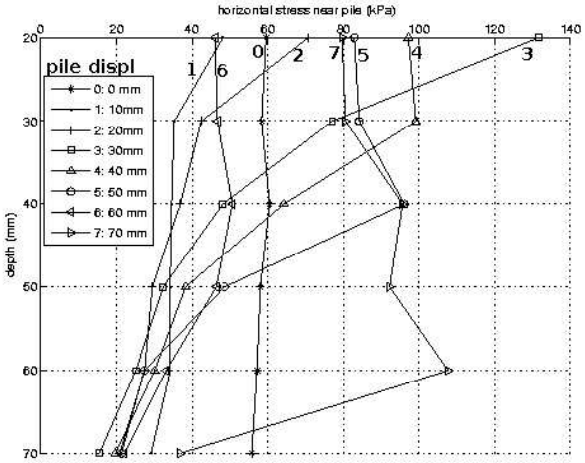

(b) Horizontal stress on virtual vertical cross section near the pile

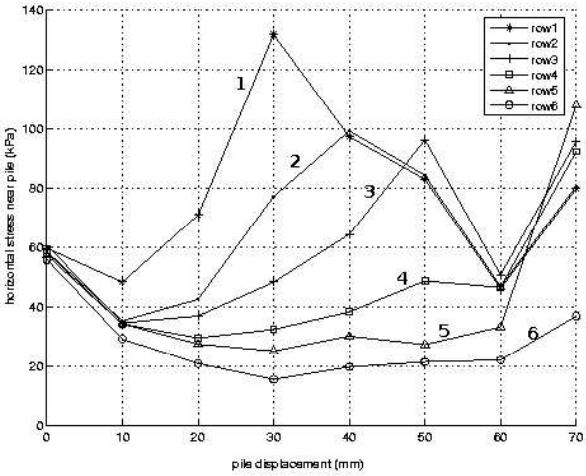

(c) Development of horizontal stress in fixed point next to the pile

Figure 3: Measured principal stress directions in particle assembly

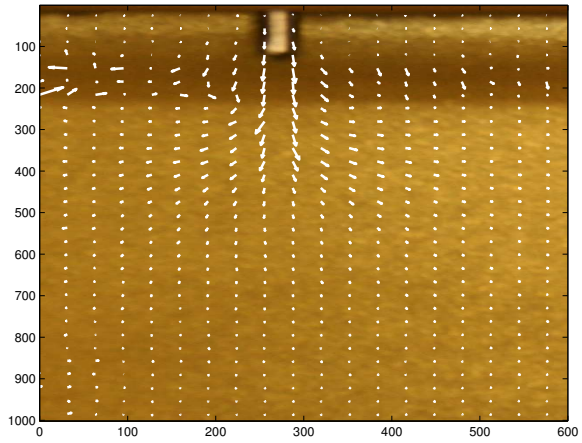

(a) displacement field, white arrows indicate displacement vectors

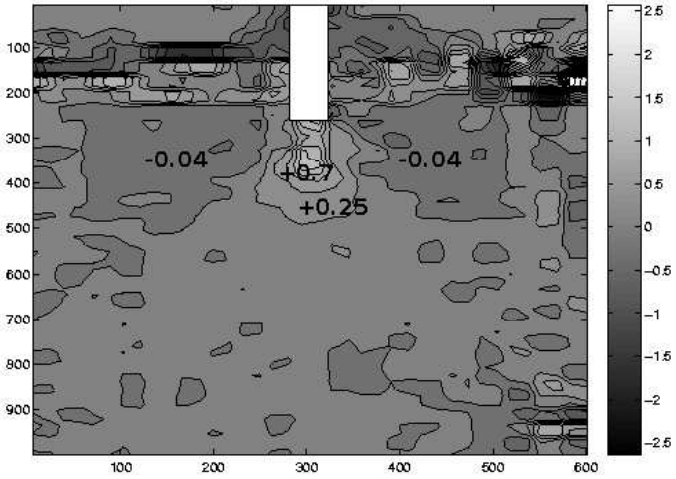

(b) volumetric strain

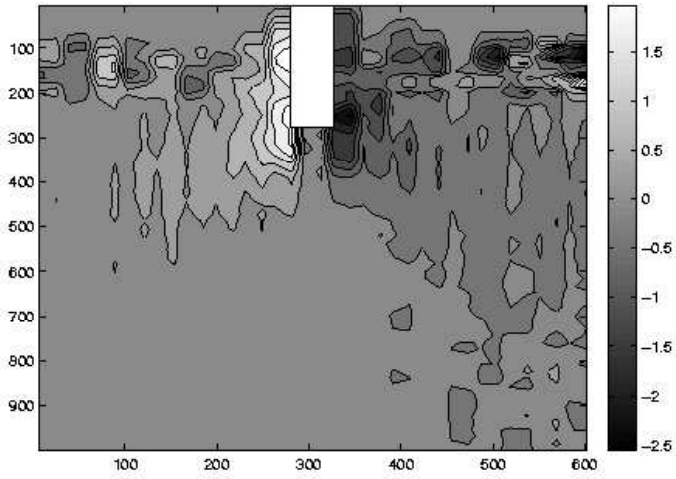

(c) shear strain

Figure 4: Measured displacement field, volumetric and shear strain in particle assembly, negative values are compressive

assemblies. The application of the surcharge is also under review. Instead of constant displacement a constant load on top of the sample is considered. Finally the test series will be extended with several more initial densities of the particle assembly.

The occurrence of large strains and non linear stress behaviour in the zone around the displacement pile suggests that numerical models capable of large strains and constitutive models which properly incorporate changes in volumetric strain and stress state should be used to predict load-settlement behaviour of the displacement pile.

6 CONCLUSIONS

The strain and stress conditions near a displacement pile have been measured in a plane strain photoelastic setup. The development of horizontal stress near the displacement pile is a complex phenomenon which is hard to quantify. When the stress is monitored in one stress point (Fig. 4(a) some evidence is found of a initial stress build-up after which a gradual decrease follows. This mechanism is supported by the measured displacement field.

The strain generated during pile installation exceeds 100 %. This results in a highly distorted zone around the pile, this zone is local, about twelf pile diameters in width. Below the pile tip a distinct dilatant soil behaviour is found.

REFERENCES

Ajovalasit, A., S. Barone, and G. Petrucci (1998). A review of automated methods for the collection and analysis of photoelastic data. *Journal of Strain Analysis 33*(2), 75–91.

Allersma, H. (1982). Determination of the stress distribution in assemblies of photoelastic particles. *Experimental Mechanics 22*(9), 336–341.

Allersma, H. (1987). *Optical analysis of stress and strain in photoelastic particle assemblies*. Ph. D. thesis, Delft University of Technology.

Allersma, H. and W. Broere (2002). Optical analysis of stress around a penetrating probe in granular material. In *Physical Modelling in Geotechnics: Proceedings of the international Conference on Physical Modelling in Geotechnics*, pp. 149–154.

Davidson, J. and A. Boghrat (1983). Displacements and strains around probes in sand. In *Proceedings of the conference on Geotechnical Practice In Offshore Engineering*, pp. 181–202.

De Pater, C. and J. Nieuwenhuis (1986). Method for measuring the deformations of a sand surface. *Géotechnique 36*(4), 581–585.

Drescher, A. (1976). An experimental investigation of flow rules for granular materials using optically sensitive glass particles. *Géotechnique 26*(4), 591–601.

Mori, N. and K. Chang (2003). Mpiv toolbox for matlab.

Sadek, S., M. Iskander, and J. Liu (2003). Accuracy of digital image correlation for measuring deformations in transparent media. *Journal of Computing in Civil Engineering 17*(2), 88–96.

Smith, I. and D. Griffiths (1998). *Programming the finite element method*. John Wiley & Sons LTD.

Sveen, J. and E. Cowen (2004). *Quantitative imaging techniques and their application to wavy flow*. World Scientific.

Wakabayashi, T. (1957). Photoelastic method for determining of stress in powdered mass. In *Proceedings of the seventh Japanese National Conference on Applied Mechanics*, pp. 153–158.

White, D. and B. Lehane (2004). Friction fatigue on displacement piles in sand. *Géotechnique 54*(10), 645–658.

Wolf, H., D. König, and T. Triantafyllidis (2003). Experimental investigation of shear band patterns in granular material. *Journal of Structural Geology 25*, 1229–1240.